Impact erosion prediction using the finite volume particle method with improved constitutive models

Sebastián Leguizamón, Ebrahim Jahanbakhsh, Audrey Maertens, Christian Vessaz, Siamak Alimirzazadeh and François Avellan

EPFL, Department of Mechanical Engineering, Laboratory for Hydraulic Machines (LMH), Avenue de Cour 33 Bis, 1007 Lausanne, CH

E-mail: sebastian.legui@epfl.ch

Abstract. Erosion damage in hydraulic turbines is a common problem caused by the high-velocity impact of small particles entrained in the fluid. In this investigation, the Finite Volume Particle Method is used to simulate the three-dimensional impact of rigid spherical particles on a metallic surface. Three different constitutive models are compared: the linear strain-hardening (L-H), Cowper-Symonds (C-S) and Johnson-Cook (J-C) models. They are assessed in terms of the predicted erosion rate and its dependence on impact angle and velocity, as compared to experimental data. It has been shown that a model accounting for strain rate is necessary, since the response of the material is significantly tougher at the very high strain rate regime caused by impacts. High sensitivity to the friction coefficient, which models the cutting wear mechanism, has been noticed. The J-C damage model also shows a high sensitivity to the parameter related to triaxiality, whose calibration appears to be scale-dependent, not exclusively material-determined. After calibration, the J-C model is capable of capturing the material's erosion response to both impact velocity and angle, whereas both C-S and L-H fail.

1. Introduction

Hydroabrasive erosion is the gradual removal of material from a surface in contact with a sediment-laden flow [1]. It can be divided in two categories: impact erosion, where the sediment particles entrained in the fluid collide with the surface, and sliding abrasion, where a bed of particles bears against the surface with a tangential velocity. The most important parameters describing impact erosion, our subject matter, are the impact angle and velocity, although other factors are also important. These include: the erodent particle material properties, size distribution, shape and concentration; the surface material properties, including microstructure; the flow characteristics such as turbulence intensity [2]. Furthermore, these parameters are deeply linked: for instance, the particle size determines the energy content of the impact, but it also determines the location, velocity and angle of the impact, given some fixed flow conditions.

Erosive wear of hydraulic turbomachines is a common problem which implies efficiency degradation, cavitation enhancement, increased vibration, outage for expensive repairs and, if left untreated, may ultimately lead to component failure [3]. Although all turbomachines are affected by erosion to a certain extent, Pelton turbines are especially vulnerable due to the high water velocity, both in the injector and against the bucket surface. Several strategies to mitigate the erosion damage in Pelton turbines exist: investing in expensive coatings, scheduling periodic repair campaigns, using more effective settling basins, designing for sediment laden

water (*e.g.* larger buckets), limiting operation during high sediment concentration periods (*e.g.* monsoon) and using specially designed materials [2–6]. Each of these strategies comes at a cost, and involves the whole hydropower station engineering: turbine design, civil works, operation strategy and maintenance scheduling. A cost-benefit approach can be used to optimize the design of a Pelton hydropower installation in terms of these strategies, but it would require a tool to predict the erosion phenomenon under specific conditions: bucket geometry, material and sediment characteristics.

The erosion phenomenon has been studied experimentally for decades. Already in the 1960s Finnie [7] investigated the erosion rate on several materials as a function of impact angle, identifying two typical modes of erosion: brittle materials erode the most at high impact angles, whereas ductile materials do so at lower angles. Bitter [8] identified two erosion mechanisms: the accumulation of plastic deformation, predominant at high impact angles, and the removal of material by cutting, effective at low impact angles. They were termed deformation and cutting wear, respectively. Beginning with these analytical models, many correlations have been proposed to predict the erosion rate under defined conditions [7–11]. These require, however, empirical case-dependent constants and are therefore limited to maintenance scheduling once they have been tuned to a specific installation [2, 4, 12]. Scale model tests have been performed to study the erosion of Pelton buckets [13, 14]. Nonetheless, the lack of scaling laws prevents the transposition to prototype scale (*e.g.* much weaker bucket material to achieve faster erosion; smaller buckets –higher curvature and thus erosion– to limit model cost). Erosion test rigs have been used to evaluate the resistance of materials to erosion and the effect of the most relevant parameters [15, 16]. Using this data to predict the erosion rate distribution on a particular turbine surface is, however, difficult because the erosion conditions (impact angle and velocity probability density distributions, functions of the sediment size) are unknown.

Numerical simulation has become the third pillar of scientific endeavor, together with analytical and experimental techniques. Although subject to empirical tuning and validation, numerical simulations can be useful where experiments are too expensive, or data is too difficult to extract. Computational Fluid Dynamics (CFD) has been used to calculate the trajectories of sediments in impinging slurry jets [17, 18], showing that the particles impact the target with a distribution of angles and velocities quite spread around the velocity and incidence angle of the jet. These investigations used empirical erosion models to reproduce the erosion patterns seen in experiments with reasonably accurate results, once their parameters have been tuned to the dataset. Noepane [19] used CFD particle tracking coupled with two standard erosion correlations to estimate the erosion in a Francis turbine. The erosion patterns are only in moderate qualitative agreement with the experimental data. Other researchers have investigated the problem from the microscopic perspective by performing simulations of explicit particle impacts both with the Finite Volume Method (FVM) [20–22] and Smoothed Particle Hydrodynamics (SPH) [23]. The advantage of such an approach is that the erosion is found by solving the governing equations of the material, rather than from an empirical correlation. Although these material models also require some experimental input, such an approach is supported by broader physics and should therefore be more general.

The present investigation is framed within a wider effort to develop an erosion prediction methodology encompassing both the sediment transport fluid dynamics problem and the microscopic particle impact erosion problem. As a first step, we investigate the effect of the material constitutive and damage models in the prediction of the erosion rate dependence on impact angle and velocity, the two leading parameters. The aforementioned investigations [20–23] have already approached this problem with a variety of material models. In this investigation we compare such models in order to establish the most appropriate one to be used with the recently developed Finite Volume Particle Method (FVPM).

2. Methodology

2.1. The Finite Volume Particle Method (FVPM)

In order to simulate the problem at hand, FVPM is used to discretize the domain. FVPM is a recently developed meshless method that takes advantage of many of the desirable features of conventional mesh-based finite volume methods, whilst still exploiting the advantages of the particle-based approach.

FVPM is based on an Arbitrary Lagrangian-Eulerian (ALE) formulation, meaning that the computational nodes may move with an arbitrary velocity. This node movement provides a natural advantage for handling moving interfaces with ease. FVPM is therefore well suited for free surface flow problems, as well as problems where high-deformations are expected such as impact simulations, where the traditional FVM suffers from excessive mesh distortion and tangling [23, 24]. Note that unlike SPH, FVPM is both locally conservative and consistent [25].

FVPM can be interpreted as a generalization of the traditional FVM [26], with moving, overlapping volumes. The flux exchange between volumes is weighted by interaction vectors, analogous to the area vectors defined on the surfaces of traditional finite volumes. The FVPM interaction vectors are calculated exactly by using sphere-supported top-hat kernel overlaps. For a detailed derivation of the 3D-FVPM formulation, its validation and application, see [25, 27, 28].

2.2. Governing Equations

The mass and linear momentum conservation equations, which are solved for the solid being eroded, are expressed as follows:

$$\frac{d\rho}{dt} + \rho \nabla \cdot \mathbf{C} = 0 \tag{1}$$

$$\rho \frac{d\mathbf{C}}{dt} = \nabla \cdot (\bar{\bar{\mathbf{s}}} - p\bar{\bar{\mathbf{I}}}) + \rho \mathbf{g} + \mathbf{f}_c \tag{2}$$

where ρ is the density, $\mathbf{C}$ is the velocity, p is the pressure, $\bar{\bar{\mathbf{s}}}$ is the deviatoric stress tensor, $\mathbf{g}$ is the gravitational acceleration, $\mathbf{f}_c$ is the contact force and $\frac{d}{dt}$ denotes the material derivative.

The pressure is obtained from the following equation of state:

$$p = a^2(\rho - \rho_\circ) \tag{3}$$

where a is the speed of sound in the solid, and $\rho_\circ$ is the initial (reference) density. The speed of sound is given by the material's Young's modulus, E, and Poisson's ratio, ν, according to:

$$a = \sqrt{\frac{E}{3\rho_\circ(1-2\nu)}} \tag{4}$$

The material is modeled as isotropic and elasto-plastic. The radial return plasticity algorithm is used: At each time step and for each particle, a trail stress is computed based on the Jaumann rate of stress; if the trail stress is greater than the yield stress, then the trail stress is scaled back to the von Mises yield surface, and an increment in plastic strain is caused.

The silt particles are modeled as spherical and rigid. Their mass and volume are constant, and their acceleration is found from Newton's second law:

$$m \frac{d\mathbf{C}}{dt} = m\mathbf{g} + \mathbf{f}_c \tag{5}$$

where m is the silt particle mass. The silt-solid contact force, $\mathbf{f}_c$, is calculated using a penalty method based on Hertz's contact theory.

2.3. Material Constitutive and Damage Models

A material constitutive model is required to close the system by establishing a relation between stress and strain. The three constitutive models studied in this investigation are presented in Table 1. The linear hardening (L-H) model only includes the effect of work hardening, *i.e.* the increase in yield strength a metal experiences when plastically deformed, due to the movement and accumulation of dislocations. Therefore the L-H model provides the yield stress, σ_y, as a function of plastic deformation, ϵ_p, and two material constants, A and B.

Both the Cowper-Symonds [29] (C-S) and the Johnson-Cook [30] (J-C) models include a non-linear work hardening term characterized by the strain hardening exponent, n. They also include the effect of strain rate: the yield strength of a material tends to increase with the rate of deformation being applied. Therefore, these constitutive equations include a second term which includes the strain rate, $\dot{\epsilon}$, and two constants, R and p. The thermal softening effect, available in the J-C model, is neglected in this investigation because, under the impact velocities studied, a negligible temperature increase is expected [31, 32].

The accumulation of plastic strain leads to material failure, in which case the affected particle is removed from the system. This occurs once the material damage, δ, reaches a value of 1.0. The cumulative damage law is written as:

$$\delta = \sum_i \frac{\Delta\epsilon_{p,i}}{\epsilon_{f,i}} \tag{6}$$

where $\Delta\epsilon_{p,i}$ is the plastic strain increment for time step i, and $\epsilon_{f,i}$ is the failure plastic strain for time step i. For the L-H and C-S models the failure plastic strain is a material constant. Therefore only the J-C model includes a damage model which is a function of strain rate, $\dot{\epsilon}$, pressure, p, von Mises equivalent stress, σ_{vm}, and four material constants, D_i. This phenomenological damage model has been proposed according to the observation that metals tend to have higher fracture strain when under hydrostatic pressure and when deformed at high velocity. The ratio of p to σ_{vm}, known as stress triaxiality, is the leading effect, followed by the strain rate [30], as revealed by the exponential and natural logarithm functions in (10).

Table 1: Material Constitutive and Damage Models.

Model Name	Yield Stress and Failure Plastic Strain Equations	
Linear Hardening (L-H)	$\sigma_y = A + B\epsilon_p$ $\epsilon_f = \text{constant}$	(7)
Cowper-Symonds (C-S)	$\sigma_y = [A + B(\epsilon_p)^n]\left[1 + \left(\frac{\dot{\epsilon}}{R}\right)^{\frac{1}{p}}\right]$ $\epsilon_f = \text{constant}$	(8)
Johnson-Cook (J-C)	$\sigma_y = [A + B(\epsilon_p)^n]\left[1 + p \cdot \ln\left(\frac{\dot{\epsilon}}{R}\right)\right]$	(9)
	$\epsilon_f = \left[D_1 + D_2\ \exp(D_3\ \frac{p}{\sigma_{vm}})\right]\left[1 + D_4 \cdot \ln\left(\frac{\dot{\epsilon}}{R}\right)\right]$	(10)

2.4. Material Characterization

The constitutive and damage model material constants need to be found experimentally. The work hardening can be characterized with a quasi-static tensile test, which renders the stress-strain curve of the material, from which the initial yield stress and the hardening law can be found. The strain rate behavior can be characterized with a Split-Hopkinson bar apparatus, which provides stress-strain curves for a range of strain rates. Data fitting is then performed to find the strain rate parameters that best match the experimental data set [33].

The J-C damage model strain rate dependence can be calibrated in a similar manner. The model dependence on triaxiality, however, cannot be found by experimental means alone because there is no analytical expression for triaxiality on arbitrary geometries. A hybrid experimental-numerical approach is necessary. Tensile tests are performed on a set of specimen geometries implying different triaxiality states; equivalent simulations are also performed with successive sets of damage model parameters $D_{1,2,3}$; the parameter set is changed until a good agreement with the experimental data is achieved over the whole set of specimen geometries (*i.e.* triaxiality states) [34].

In spite of being two of the most widespread models, both J-C and C-S have important shortcomings. For instance, it has been found that the model parameters change very significantly depending on the experimental apparatus used to characterize the material (*e.g.* Split-Hopkinson bar in compression; Split-Hopkinson bar in shear; Taylor impact test) [24]. Furthermore, agreement between experiments and simulations tends to be poor, especially when the problem involves strain rate and triaxiality states exceeding the range used in the material characterization [30]. A scale dependence has also been evidenced in the J-C damage model calibration, possibly due to size-dependent failure modes [34]. These circumstances point to the fact that the model parameters are not really material constants, but barely a phenomenological approximation to complex microscopic interactions.

2.5. Case Description

The current investigation involves only the solid material being impacted by edorent particles; the transport of the sediments by the fluid is not considered at this stage, but will be handled later on. The material studied is the titanium alloy Ti-6Al-4V. It has been chosen because, unlike the typical hydro turbine stainless steel, the model parameters can be found in literature, as well as experimental and numerical studies of its erosion behavior. The erodents are rigid spherical silicon carbide particles with a diameter of 100 μm, following the experimental case [15]. Indeed, hydroabrasive erosion typically involves particles in the range of 50 to 300 μm [3].

The case discretization is presented in Figure 1. The specimen is comprised of three levels of refinement around the impact location, where the particle diameter is 5.3 μm following a convergence analysis performed beforehand. The contact between erodent particles is neglected in order to speed up the simulations by allowing more frequent impacts.

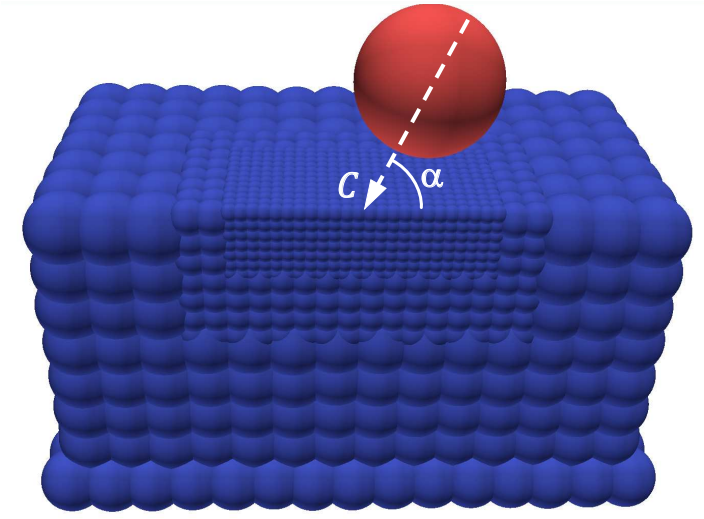

Figure 1: Case discretization by FVPM. Only half of the domain is shown. The impact is defined by angle α and velocity magnitude C.

Table 2: Material Properties and Model Constants for Ti-6Al-4V [21, 33, 34].

Property	Value
Density, $\rho_\circ$ [kg m^{-3}]	4428
Young's modulus, E [GPa]	120
Poisson's ratio, ν [−]	0.31
Initial yield stress, A [MPa]	1098
Hardening base, B [MPa]	1092
Hardening exponent, n [−]	0.93
C-S's p, [−]	9.0
C-S's R, [s^{-1}]	120
J-C's p, [−]	0.014
J-C's R, [s^{-1}]	1.0
J-C's D_1, [−]	−0.09
J-C's D_2, [−]	0.27
J-C's D_3, [−]	0.48
J-C's D_4, [−]	0.014

The erosion rate is defined as the slope of the accumulated erodent mass *vs.* accumulated eroded mass curve. Such a curve is only linear after an initial period of incubation during which plastic deformation accumulates on the surface of the specimen. The average number of impacts on a given spot before the steady erosion rate is reached can be estimated from the experimental reference [15] to be of the order of one hundred. Indeed, the simulations only reached such a steady state after 80 to 200 impacts, depending on the impact angle. Note that this is in sharp contrast with previous numerical investigations which claim to predict the steady erosion rate after only five [23] to ten [20] impacts.

3. Results and Discussion

The steady erosion rate as a function of impact angle is presented in Figure 2 for the three models studied, as well as two experimental references. It is clear that the L-H model greatly overpredicts the removal of material. Indeed, both C-S and J-C predict an erosion rate almost one order of magnitude smaller, closer to the experimental value. To understand this, in Figure 3 we present the average plastic work density (the area under the plastic part of the stress-strain curve, *i.e.* the total energy absorbed by the material before failure) for the three models. It becomes clear that the predicted erosion rate is directly linked to the energy absorption capacity of the material. Furthermore, strain rate dependence is evidenced by the fact that both C-S and J-C predict angle-dependent plastic work density. Not surprisingly, the higher normal velocity component at normal impact angle implies a larger strain rate and a tougher material response.

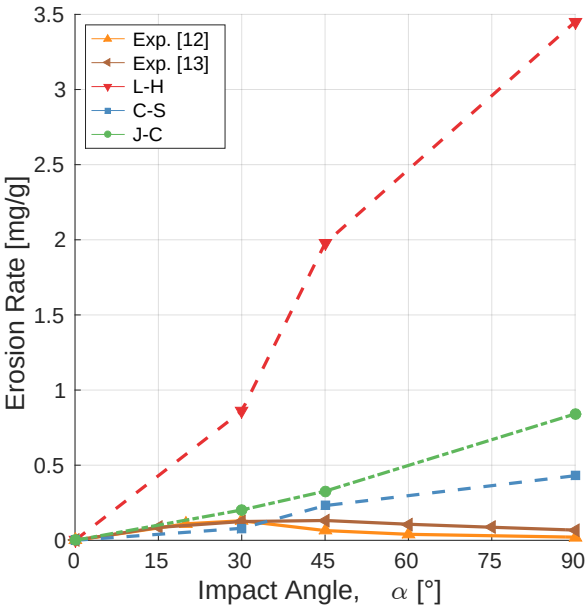

Figure 2: Erosion rate for the three models and two experimental studies. $C = 55$ [m s^{-1}].

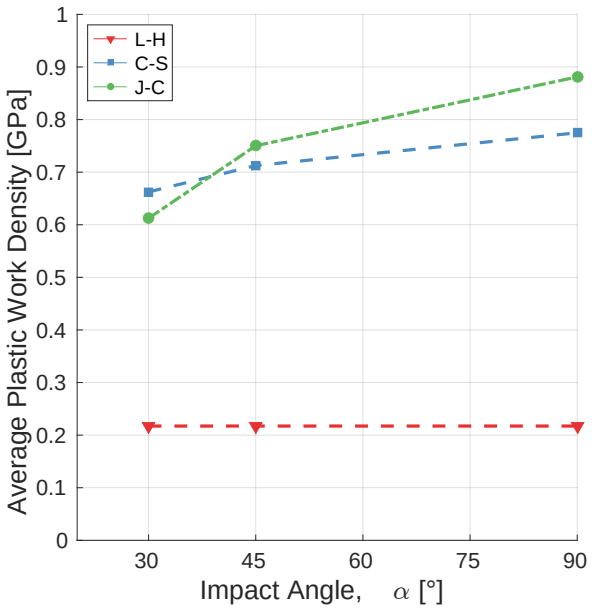

Figure 3: Average plastic work density at failure for the three models studied. $C = 55$ [m s^{-1}].

It is interesting to note that, in spite of the very different formulations of the C-S and J-C models, their response in terms of energy absorption is very similar as seen in Figure 3. Indeed, the C-S model is very sensitive to the strain rate given the power relation used in (8). This is evident in Figure 4 in which the average ultimate stress at failure is illustrated. The J-C model predicts a much milder increase in strength due to the logarithmic dependence on strain rate compared with C-S, whereas the L-H model accounts for no variation in yield strength with impact angle at all. The average plastic strain at failure is presented in Figure 5. J-C is the only model which predicts high failure strains, owing to its triaxiality and strain rate dependent damage model. On the contrary, neither L-H nor C-S includes a damage model, so their failure

plastic strain is a material constant fixed at 0.18. What is interesting is that J-C and C-S converge to a similar behavior energy-wise: the significant increase in strength predicted by C-S is compensated by a simultaneous increase in strength and failure strain in J-C.

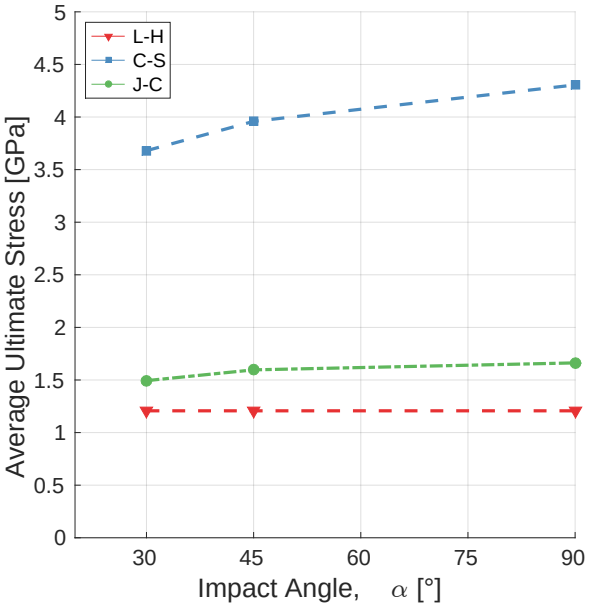

Figure 4: Average ultimate stress for the three models studied. $C = 55$ [m s^{-1}].

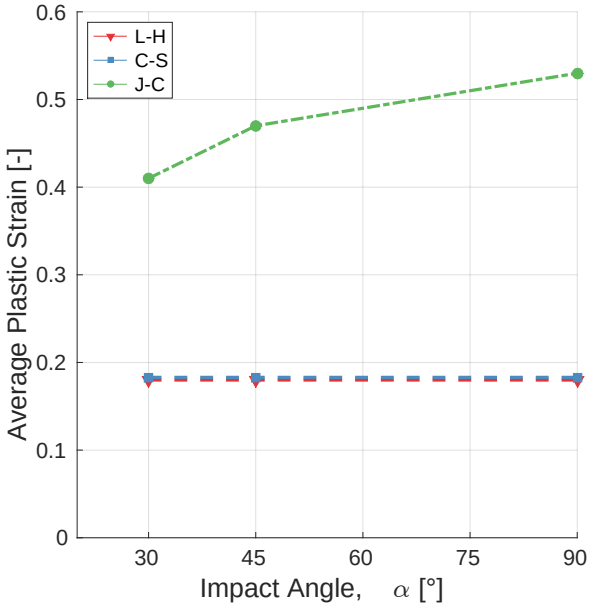

Figure 5: Average plastic strain at failure for the three models studied. $C = 55$ [m s^{-1}].

The energy absorbed by the material before failure is not the only parameter that explains the magnitude of the erosion rate. Indeed, note that both C-S and J-C predict increasing energy absorption with increasing impact angles, Figure 3, although the erosion rate predicted also increases with the angle, Figure 2. This is explained by the fact that the portion of the erodent particle impact energy transferred to the material is not fixed, but depends on the impact angle. Analyses of the results, not presented here for lack of space, show that at low incidence angle, the low perpendicular velocity causes mostly elastic deformation in the material, leading to almost no plastic deformation and the erodent particle conserving most of its initial kinetic energy. This implies a very low erosion rate, in spite of the fact that the energy absorption capacity of the material is predicted to be lower at low impact angles.

In order to extract energy from the parallel motion of the incident erodent particle a simple Coulomb kinetic friction model of the form $\mathbf{f}_f = \mu \mathbf{f}_n$ has been implemented, where the friction force opposing movement, $\mathbf{f}_f$, is proportional to the force applied normal to the surface, $\mathbf{f}_n$. Other researchers have found it necessary to tune the friction coefficient, μ, in order to accurately predict the outcome of particle impact simulations [24], and it might even be necessary to vary μ with α, even increasing μ two-fold for low impact angles [31].

The steady erosion rate for several values of the friction coefficient is shown in Figure 6. Only the C-S and J-C models are conserved since the L-H model has been shown to be incapable of accounting for our high strain rate problem. The results show that the erosion rate at low angles is greatly increased compared to the frictionless simulations. Only deformation wear is caused if friction is neglected: the cutting mechanism of erosion, dominant at low impact angles, relies on having an adequate friction model. As such, the model does not represent the typical interaction between flat surfaces; instead it is supposed to capture the cutting wear mechanism. A friction coefficient of 1.0 is therefore not unrealistic, it corresponds to the condition where the force required to cut through the material is equal to the force required to penetrate it. Being related to the cutting mechanism, μ probably depends on the particle shape (sharpness) and hardness.

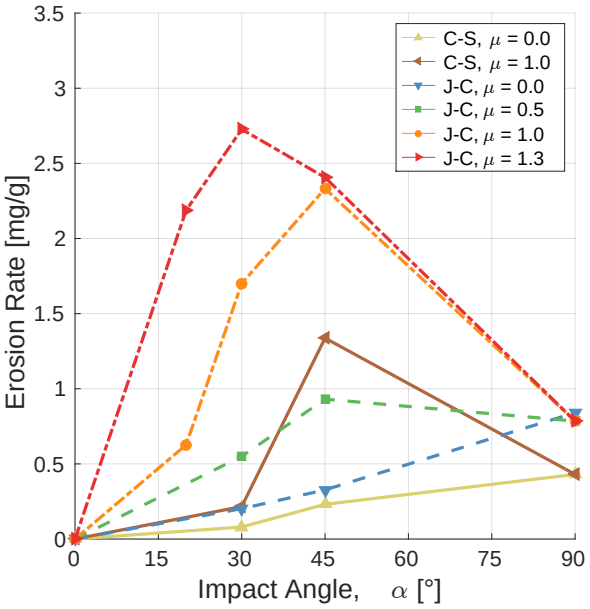

Figure 6: The effect of the friction coefficient on the erosion rate. $C = 55$ [m s^{-1}].

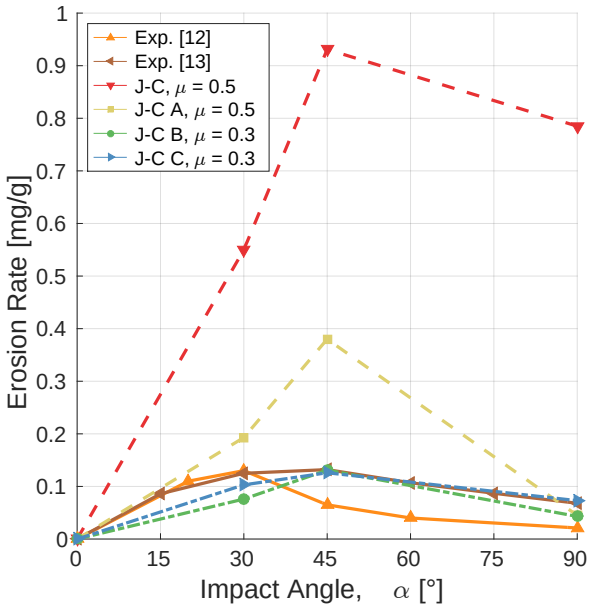

Figure 7: The effect of the J-C damage model parameters on the erosion rate. $C = 55$ [m s^{-1}].

Even though the use of a friction model allows to better capture the erosion rate trend, which is maximum at low impact angle, the magnitude is still far from the experimental value. Noticing the fact that the J-C damage model has shown a scale-dependence, where the failure parameters derived from a scaled-down testing procedure would not be suitable for use on a full-scale test [34], it has been decided to study the sensitivity of the erosion rate to the damage model parameters. The C-S model is incapable of capturing the erosion phenomenon adequately because of a lack of damage model, neglecting triaxiality altogether. Furthermore, as seen in Figure 6, its response to the friction coefficient is much less consistent that the J-C model response. Only the J-C model is therefore conserved hereafter.

We have followed the standard procedure of performing simulations for a set of triaxiality states while varying $D_{1,2,3}$ until a satisfactory agreement with experiment is achieved [34]. The set of triaxiality states is given by the impact angles, since it has been found that at higher incidence the pressure dominates, whereas at lower angles the shear caused by the parallel erodent motion dominates. In other words, it has been found that triaxiality increases with increasing impact angle. The erosion rate for several combinations of the parameters $D_{2,3}$ (sets A, B and C) is presented in Figure 7. The parameters are those found in Table 2, except for: $D_{3,A} = 0.96$, $D_{3,B} = 1.2$, $D_{2,C} = 0.20$ and $D_{3,C} = 1.5$. Increasing the model sensitivity to triaxiality increases the failure strain, especially at higher impact angle, leading to a much better agreement with the experimental results. It can be argued that the original damage model parameters might not be adequate to simulate the material behavior at the very small scales involved in sand erosion, and that finding an adequate set $D_{1,2,3}$ is therefore necessary.

The results of the J-C model with parameter set B shows a reasonable agreement with the experimental results, even though only D_3 has been changed. They predict a maximum erosion rate at 45°, in agreement with one of the experiments [16] and two other numerical investigations [21, 23]; other experimental results [15] show a higher erosion rate at 30°. Although a better calibration could be performed, note that the simulation results are not expected to match the experimental results exactly, since they are not equivalent: When performing a sand blasting experiment, even though the air jet is oriented perpendicular to the target, about half the particles impact at less than 80° [35] because they tend to follow the deviated air stream.

Similarly, when using a water jet, as many as 80% of the particles impact at less than 80°, and with a velocity about half the jet velocity [18]. It is reasonable to expect a similar behavior with other impact angles. For this reason, to fully calibrate the material model, the coupled sediment transport - material erosion problem must be simulated and compared to equivalent experimental erosion rate results.

The second governing parameter is the impact velocity, which has been found to follow a power law, with metals exhibiting an exponent in the range of 2.0 to 3.4 [1]. In Figure 8 we present the erosion rate for a range of impact velocities using the J-C model with the original constants as well as sets B and C. It is encouraging to see that the results of both J-C B and C are in much closer agreement with the experimental velocity exponent (2.35 [15]), even though the calibration has been performed to fit the angle curve without ever performing any test for the velocity dependence. This points to the fact that calibrating the triaxiality dependence brings the model closer to the real material behavior, rather than just fitting the data.

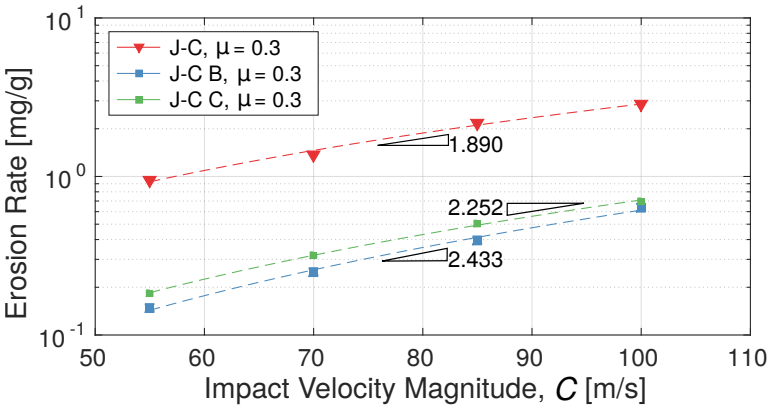

Figure 8: The effect of velocity on erosion rate at an angle of 45°. The slope of the curve represents the exponent in the power law describing the velocity dependence. Other numerical investigations have found values of 2.269 [20] and 2.337 [23], with the experimental value being about 2.35 [15].

4. Conclusion

Three constitutive models have been assessed for the problem of erosion prediction using FVPM. The Johnson-Cook model has been found to be the most appropriate one, since it accounts for strain rate and triaxiality, both of which are paramount characteristics.

First, it has been shown that a model accounting for strain rate is indispensable, since the material response is significantly tougher at the very high strain rate regime of the problem at hand. It has also been shown that both the Cowper-Symonds and Johnson-Cook models predict similar angle dependence for the energy absorption capacity of the material, in spite of rather different formulations.

The need for a friction model to account for the cutting wear mechanism present at low impact angles has been evidenced. A high sensitivity to the friction coefficient has been shown, pointing to the need of calibrating it to adequately capture the energy extraction from the impacting particles. The Johnson-Cook damage model also shows a high sensitivity to the triaxiality parameter. A calibration of such parameter is needed, presumably because it is not exclusively material dependent, but scale dependent as well.

Finally, it has been shown that a complete fluid dynamics - solid mechanics simulation is required to adequately calibrate the material model by comparison to equivalent experimental results. Future work will focus on coupling the FVPM fluid and solid solvers in an efficient way, to then calibrate the material model for martensitic stainless steel.

Acknowledgments

The authors would like to thank General Electric Power - Hydro for their financial support and technical assistance, as well as the Swiss Commission for Technology and Innovation (CTI), which has financially supported this project with grant No. 17568.1.

References

[1] Preece C M and Macmillan N H 1977 *Ann. Rev. Mater. Sci.* **7** 95–121

[2] Duan C G, Karelin V Y, Brekke H, Wu L, Matsumura M, Chen B, Denisov A I and Cai Y 2002 *Abrasive Erosion and Corrosion of Hydraulic Machinery* (*Series on Hydraulic Machinery* vol 2) ed Duan C G and Karelin V Y (London: Imperial College Press)

[3] Grein H and Schachenmann A 1992 *Water Power and Dam Construction* 19–24

[4] Padhy M K and Saini R P 2008 *Renewable and Sustainable Energy Reviews* **12** 1974–87

[5] Bajracharya T R, Acharya B, Joshi C B, Saini R P and Dahlhaug O 2008 *Wear* **264** 177–84

[6] Karimi A, Verdon C, Martin J and Schmid R 1995 *Wear* **186-187** 480–6

[7] Finnie I 1960 *Wear* **3** 87–103

[8] Bitter J G A 1963 *Wear* **6** 5–21

[9] Hutchings I M 1974 *Wear* **27** 121–8

[10] Hutchings I M 1992 *J. Phys. D: Appl. Phys.* **25** 212–21

[11] Finnie I, Stevick G R and Ridgely J R 1992 *Wear* **152** 91–8

[12] Thapa B S, Thapa B and Dahlhaug O G 2012 *Energy* **41** 386–91

[13] Padhy M K and Saini R P 2011 *Energy* **36** 141–7

[14] Padhy M K and Saini R P 2012 *Energy* **39** 286–93

[15] Yerramareddy S and Bahadur S 1991 *Wear* **142** 253–63

[16] Avcu E, Yildiran Y, Sahin A, Fidan S and Sinmazelik T 2014 *Acta Physica Polonica A* **125** 541–543

[17] Wang M H, Huang C, Nandakumar K, Minev P, Luo J and Chiovelli S 2009 *International Journal of Computational Fluid Dynamics* **23** 155–72

[18] Sugiyama K, Harada K and Hattori S 2008 *Wear* **265** 713–20

[19] Neopane H P 2010 Ph.D. thesis Norwegian University of Science and Technology

[20] Wang Y F and Yang Z G 2008 *Wear* **265** 871–8

[21] Kumar N and Shukla M 2012 *J. Comput. Appl. Math.* **236** 4600–10

[22] Balu P, Kong F, Hamid S and Kovacevic R 2013 *Tribology International* **62** 18–28

[23] Wang Y F and Yang Z G 2009 *Tribology International* **42** 373–7

[24] Takaffoli M and Papini M 2012 *Wear* **274** 50–9

[25] Jahanbakhsh E, Vessaz C, Maertens A and Avellan F 2016 *Comput. Methods Appl. Mech. Engrg.* **298** 80–107

[26] Junk M 2003 *Meshfree Methods for Partial Differential Equations* (*Lecture Notes in Computational Science and Engineering* vol 26) ed Griebel M and Schweitzer M (Springer Berlin Heidelberg)

[27] Vessaz C, Jahanbakhsh E and Avellan F 2015 *Journal of Fluids Engineering* **137** 074501

[28] Jahanbakhsh E, Vessaz C and Avellan F 2013 *IOP Conf. Series: Earth and Environmental Science* **22** 052015

[29] Cowper G R and Symonds P S 1958 Strain hardening and strain rate effects in the impact loading of cantilever beams Tech. rep. Brown University, Div. of Appl. Mech.

[30] Johnson G R and Cook W H 1985 *Engineering Fracture Mechanics* **21** 31–48

[31] Molinari J F and Ortiz M 2002 *Int. J. Impact Eng.* **27** 347–58

[32] Yildirim B, Muftu S and Gouldstone A 2011 *Wear* **270** 703–13

[33] 2000 Experimental investigation of material models for Ti-6Al-4V titanium and 2024-T3 aluminum Tech. rep. Laurence Livermore National Laboratory

[34] 2003 Failure modeling of titanium 6Al-4V and aluminum 2024-T3 with the Johnson-Cook material model Tech. rep. Laurence Livermore National Laboratory

[35] Grewal H S, Singh H and Yoon E S 2015 *Wear* **332** 1111–9